THE JOURNAL OF PHYSICAL CHEMISTRY C
A JOURNAL OF THE AMERICAN CHEMICAL SOCIETY

pubs.acs.org/JPCC
Article

Balancing the Push–Pull Effect on the Synthesis and Fluorescent Properties of New ESIPT Dyes for Thin Film Applications

Franciela Arenhart Soares,* Guillermo Martinez-Denegri, Luis Andre Baptista, Piotr Ślęczkowski,* and Alexander Steinbüchel

Cite This: J. Phys. Chem. C 2023, 127, 17624–17636
Read Online

ACCESS | Metrics & More | Article Recommendations | Supporting Information

ABSTRACT: The development of functional materials exploiting excited-state intramolecular proton transfer (ESIPT) requires a deep understanding of the push–pull balance on their reactivity, emission mechanism, and response to the surrounding environment. In this study, we focused on the model 2-(2-hydroxyphenyl)benzothiazole (HBT) core, and we have developed a simplified synthetic pathway to obtain two new ESIPT dyes with amide groups at the para or meta positions of the phenolic ring. We studied the impact of the geometry of the push–pull system for the two HBT isomers, unraveling that it strongly influenced their reactivity patterns and fluorescence emission. The ESIPT emission of the new molecules in the solution was affected by the solvent polarity, transitioning from pure keto to pure enol emission as the solvent polarity was increased. In the spin-coated films, the intermolecular interactions generated by the push–pull balance and the molecular shape of the deposited materials were also found to be essential for defining their morphology and the related emissive properties. Furthermore, these features were tuned by applying thermal annealing or by changing the solvent used for thin film deposition. The combination of both strategies was employed to provide a more favorable molecular ordering and to increase the fluorescence quantum yield of the neat films by 150%.

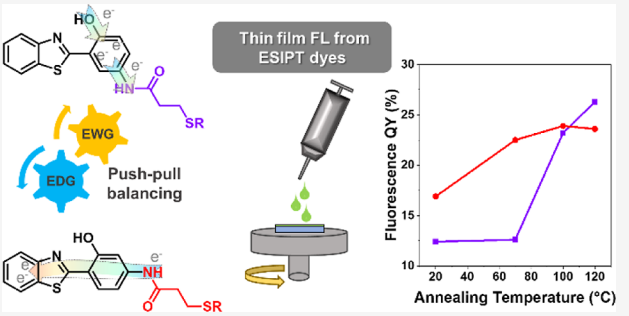

INTRODUCTION

Excited-state intramolecular proton transfer (ESIPT) is a well-known photochemical process where an enol–keto tautomerization occurs in the excited state. Mechanistically, the ESIPT process occurs in four steps: first, the enol (E) species is promoted to an excited state upon photoexcitation (E*). Then, a proton transfer occurs between a proton donor and an acceptor, forming a new excited keto (K*) tautomer. By radiative decay, the K* species goes to the ground state (K). The E species is regenerated after a reverse proton transfer in the ground state. As a consequence of the proton transfer in the excited state, ESIPT dyes show low energy fluorescence emission (FL) characterized by large Stokes shifts (~10,000 cm^{-1}).[1,2]

Considering molecules that undergo ESIPT emission, 2-(2-hydroxyphenyl)benzothiazole (HBT) derivatives have been studied extensively due to their facile, scalable, and straightforward synthesis in addition to the broad scope of applications. Benzothiazole is a strong electron-withdrawing group (EWG) which works as an acceptor, while the phenol ring plays the role of a donor in the ESIPT process.[3] In general, synthetic modifications are the commonest way to improve the emission properties of HBT derivatives by extending the conjugation length,[4] connecting bulky groups or side chains,[5] combining with other chromophores,[6] or forming complexes.[7] Substitutions are often chosen to tune emission color without drastic changes in the FL in the solid state.[8] Numerous reports are dedicated to describe synthetic modifications of the HBT core which can efficiently adjust the emission range according to the desired application or increase the quantum yield (QY) in the solution and solid state. However, those modifications are often structurally complex and require special reaction conditions, like an inert atmosphere or microwave assistance, for example.[9−11] In addition, the poor solubility of the final compounds and challenging purifications often contribute to limiting their practical applications.

Stefani et al. reported HBT derivatives bearing amino groups in the para or meta positions to the hydroxyl group. The compounds showed great dependence between the FL and the amino position since it is a strong electron donating group (EDG) to the phenolic ring and hence affects the push–pull balance of the molecule.[12] A recent theoretical study investigated the effects caused by the presence of amino

Received: July 6, 2023
Revised: August 9, 2023
Published: August 23, 2023

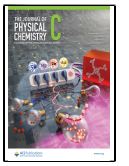

https://doi.org/10.1021/acs.jpcc.3c04543
J. Phys. Chem. C 2023, 127, 17624–17636

groups in different positions on the ESIPT mechanism.[13] Although the presence of amino groups expands new synthetic possibilities through simple reactions like acylations, nucleophilic substitutions, and others that can be conducted in one-step synthesis, further functionalization and the comparison of the para and meta isomers remain unexplored.

Due to its unique features, the ESIPT process has been extensively employed as a strategy to build fluorescent compounds with several applications like imaging agents,[14] molecular probes,[15] photonic,[16−18] optoelectronics,[19−22] and mechanochromic[23] luminescent materials. Such applications require detailed knowledge of the fluorescent properties of the material. However, little has been discussed about how the EDG and EWG balance can influence the photophysical properties in solution and the solid state of para and meta isomers. Moreover, many of the solid-state applications require materials processing and thin film fabrication for further integration in real-life devices. Importantly, following this approach, materials must be compatible with various deposition methods, and their functional properties should be studied in thin films as the ultimate form.

Postprocessing of organic thin films, like thermal or solvent vapor annealing, was demonstrated to alter the material's photophysical properties, although rarely enhancing their QY.[24−28] Most of these changes are related to morphological changes, which might also be affected by other factors such as the fabrication method, parameters, or environmental conditions. In terms of ESIPT molecules, very few studies have been performed to analyze the effect of temperature or other extrinsic conditions on the emission properties of thin films. In particular, temperatures above room temperature were reported to induce a change in the FL of the ESIPT emission, but these studies were performed either in solution or the bulk solid state (i.e., powder or crystal).[29−31] To the best of our knowledge, the effect of thermal annealing on ESIPT thin films has not been studied, which, together with morphological analysis, is of relevant interest for different applications such as optoelectronic or photovoltaic devices.

In this work, we report on the synthesis and photophysical properties of two new amide-HBT derivatives, which were obtained by amino group acylation at the para or meta positions to the phenolic group in a simple two-step procedure. By detailed studies of the materials' properties regarding the side-group position, we found that both reactivity and photophysical properties are significantly influenced by the push−pull effects caused by the EDG and EWG groups constituting para and meta isomers. The position of the amino group considerably affects its nucleophilicity, which favors its reactivity in the case of para isomers. By exploring the photophysical properties in solution including screening distinct solvent polarities, we characterize in detail the absorption and emission properties of both isomers. For both compounds, the emission shifted from pure K* in non-polar solvents to only E* in polar media, which highlights the sensitivity of the synthesized materials to the environment. The amino group acylation provides suitable materials for thin film fabrication through the solution process. The effect of thin films' thermal annealing was analyzed, revealing significant differences in the progress of absorption and FL properties of the meta and para isomers, which was in accordance with the electron density contribution for each case. Moreover, the combination of the solvent employed for the solution process and thin film thermal annealing, determines the highest QY enhancement of the studied thin films, establishing an uncommon strategy for the performance optimization of ESIPT solid-state materials.

EXPERIMENTAL SECTION AND THEORY

General. All solvents used in the experiments were purchased from Chempur (Poland) and were used without any further purification, unless specified in the procedure. Purification of products by column chromatography was carried out on silica gel (60 Å, 70−230 mesh) or in silica gel for flash chromatography (40−63 μm). Analytical thin-layer chromatography (TLC) was conducted on aluminum plates of silica gel with fluorescent pigment 60F-254. All reagents were purchased from Merck or Fisher Chemicals with at least 98% of purity. Absorption spectra in the IR range were collected using an FT-IR spectrometer, Nicolet iS50, Thermo Fisher Scientific (USA), equipped with an attenuated total reflectance (ATR) accessory with a diamond crystal. NMR experiments were recorded in BRUKER AVANCE II PLUS 700 MHz or in JEOL JNM-ECZL 400 MHz. All NMR spectra were plotted as received from the analytical department. High-resolution mass spectrometry (HRMS) measurements were performed using the Synapt G2-Si mass spectrometer (Waters) equipped with an ESI source and quadrupole-time-of-flight mass analyzer. The mass spectrometer was operated in the positive ion detection mode. The optimized source parameters were: a capillary voltage of 3.2 kV, a cone voltage of 30 V, a source temperature of 110 °C, a desolvation gas (nitrogen) flow rate of 600 L/h with a temperature of 350 °C, and a nebulizer gas pressure of 6.5 bar. To ensure accurate mass measurements, data were collected in the centroid mode, and mass was corrected during acquisition using leucine enkephalin solution as an external reference (Lock-SprayTM), which generated a reference ion at m/z 556.2771 Da ($[M - H]^+$) in the positive ESI mode. The results of the measurements were processed using the MassLynx 4.1 software (Waters) incorporated with the instrument.

Synthesis. *4-Amino-2-(benzo[d]thiazol-2-yl)phenol (**1a**).* In a round-bottom flask equipped with a magnetic bar were added *o*-thioaminobenzene (0.98 mL, 9.2 mmol), 5-aminosalicylic acid (1.416 g, 9.2 mmol), and 10 g of polyphosphoric acid. The mixture was stirred for 4 h at 180 °C, as previously described in the literature. After this time, the reaction was cooled to room temperature and the viscous mixture was diluted with water. The aqueous solution with a gray solid was neutralized with $NaHCO_3$ 10% until all solids became green.[12,32] The solid was filtered, dried overnight at 40 °C, and then crystallized from chloroform. Dark-green crystals, 87% yield. ^{1}H NMR (700 MHz, $CDCl_3$): δ 11.95 (s, 1H), 8.00 (dd, J = 8.1, 0.6 Hz, 1H), 7.93−7.90 (m, 1H), 7.54−7.50 (m, 1H), 7.44−7.40 (m, 1H), 7.04 (d, J = 2.7 Hz, 1H), 6.98 (d, J = 8.7 Hz, 1H), 6.83 (dd, J = 8.7, 2.7 Hz, 1H), 3.53 (s, 2H).

*5-Amino-2-(benzo[d]thiazol-2-yl)phenol (**1b**):* The meta compound was synthesized following the same procedure but employing 4-aminosalicylic acid (1.416 g, 9.2 mmol).[12,32] The dark-yellow solid was crystallized from chloroform. Brown crystals, 73 % yield. ^{1}H NMR (700 MHz, $CDCl_3$): δ) δ 12.66 (s, 1H), 7.92− 7.89 (m, 1H), 7.87− 7.85 (m, 1H), 7.50−7.45 (m, 2H), 7.37− 7.34 (m, 1H), 6.35 (d, J = 2.2 Hz, 1H), 6.29 (dd, J = 8.4, 2.3 Hz, 1H), 4.05 (s, 2H).

*3-((tert-Butoxycarbonyl)thio)propanoic Acid (**2**).* The compound was prepared as described in the literature.[33] To a solution of 3-mercaptopropionic acid (MPA) (200 μL, 2.3

https://doi.org/10.1021/acs.jpcc.3c04543
J. Phys. Chem. C 2023, 127, 17624−17636

mmol) in THF were added Boc_2O (600 mg, 2.7 mmol) and triethylamine (640 μL, 4.6 mmol). The reaction mixture was stirred for 36 h at room temperature. After the reaction was completed, THF was removed from the rotatory evaporator, and 1.2 mL of HCl 1 M was added to the residue. The previous solution was extracted three times with 3 mL of DCM, dried over anhydrous $MgSO_4$, and concentrated. The crude was checked by ^{1}H NMR and used without additional purification. If the crude was not pure, the workup was repeated. Colorless oil, 40% yield. ^{1}H NMR (700 MHz, $CDCl_3$): δ 3.05 (t, *J* = 7.1 Hz, 2H), 2.71 (t, *J* = 7.1 Hz, 2H), 1.51 (s, 9H).

*S-(3-((3-(Benzo[d]thiazol-2-yl)-4-hydroxyphenyl)amino)-3-oxopropyl) O-(tert-Butyl)carbonothioate (**3a**).* To a solution of the protected MPA (200 mg, 0.96 mmol) in dry DCM cooled to 0 °C in an ice bath were added DCC (201 mg, 0.96 mmol) and DMAP (11.8 mg, 0.096 mmol). Then, dye **1a** (235 mg, 0.96 mmol) dissolved in 4 mL of DCM was added dropwise. The reaction was left stirring at 0 °C for half an hour and then at r.t. until the completion of the reaction was observed by TLC using DCM and AcOEt as the eluent in the proportion 9:1. After the completion of the reaction, the resulting urea was filtered and washed with DCM. The solution was washed with 15 mL of HCl 1 M, 15 mL of $NaHCO_3$ 10%, and brine. The organic layer was dried over anhydrous $MgSO_4$, filtered, and concentrated under reduced pressure. The crude product was purified by column chromatography using DCM and AcOEt or $CHCl_3$ and acetone as the eluent in the proportion 96:4. White solid, 80% yield. FT-IR (ATR, cm^{-1}): ν 3266; 2919; 2848; 1696; 1643; 1507; 1123. ^{1}H NMR (700 MHz, $CDCl_3$): δ 12.45 (s, 1H), 8.14 (d, *J* = 2.5 Hz, 1H), 8.02 (d, *J* = 8.1 Hz, 1H), 7.94 (d, *J* = 7.9 Hz, 1H), 7.54 (t, *J* = 7.2 Hz, 1H), 7.44 (t, *J* = 7.1 Hz, 1H), 7.38−7.34 (m, 2H), 7.09 (d, *J* = 8.8 Hz, 1H), 3.20 (t, *J* = 7.0 Hz, 2H), 2.79 (t, *J* = 7.0 Hz, 2H), 1.54 (s, 9H). ^{13}C NMR (176 MHz, $CDCl_3$): δ 169.5, 168.9, 154.9, 151.8, 132.8, 129.8, 126.7, 125.6, 125.3, 122.2, 121.6, 120.0, 118.2, 116.5, 85.3, 38.0, 28.2, 26.6. HRMS-ESI calcd $[M - H]^+$ 431.1099; found, 431.1098.

*4-Amino-2-(benzo[d]thiazol-2-yl)phenyl 3-((tert-Butoxycarbonyl)thio)propanoate (**4a**).* The product was obtained as a side product of the synthesis of **3a**. Pale-yellow oil, 43% yield. FT-IR (ATR, cm^{-1}): ν 3460; 3365; 2975; 2922; 1757; 1695; 1107. ^{1}H NMR (700 MHz, $CDCl_3$): δ 8.10 (d, *J* = 8.1 Hz, 1H), 7.94 (d, *J* = 7.6 Hz, 1H), 7.59 (d, *J* = 2.8 Hz, 1H), 7.54−7.49 (m, 1H), 7.44−7.40 (m, 1H), 7.06 (d, *J* = 8.6 Hz, 1H), 6.81 (dd, *J* = 8.6, 2.8 Hz, 1H), 3.83 (s, 2H), 3.23−3.19 (m, 2H), 3.17−3.12 (m, 2H), 1.54 (s, 9H). ^{13}C NMR (176 MHz, $CDCl_3$): δ 170.6, 168.8, 162.7, 152.9, 144.7, 140.3, 135.4, 126.3, 126.3, 125.3, 124.4, 123.3, 121.4, 117.9, 115.3, 85.1, 35.6, 28.2, 25.8. HRMS-ESI calcd $[M - H]^+$ 431.1099; found, 431.1097.

*S-(3-((4-(Benzo[d]thiazol-2-yl)-3-hydroxyphenyl)amino)-3-oxopropyl) O-(tert-Butyl)carbonothioate (**3b**).* To a solution of the protected MPA (200 mg, 0.96 mmol) in dry DCM cooled to 0 °C in an ice bath were added the DCC (201 mg, 0.96 mmol) and HOBt (161 mg, 1.05 mmol). Then, dye **1a** (235 mg, 0.96 mmol) dissolved in 4 mL of DCM was added dropwise. The reaction was left stirring at 0 °C for half an hour and then at r.t. until the completion of the reaction was observed by TLC using DCM and AcOEt as the eluent in the proportion 9:1. After the completion of the reaction, the resulting urea was filtered and washed with DCM. The solution was washed with 15 mL of HCl 1 M, 15 mL of $NaHCO_3$ 10%, and brine. The organic layer was dried over anhydrous $MgSO_4$, filtered, and concentrated under reduced pressure. The crude product was purified by column chromatography using DCM and AcOEt or $CHCl_3$ and acetone as the eluent in the proportion 98:2. White solid, 61% yield. FT-IR (ATR, cm^{-1}): ν 3335 3211; 2977; 1692; 1603; 1526; 1390. ^{1}H NMR (700 MHz, $CDCl_3$): δ 12.62 (s, 1H), 7.95 (d, *J* = 8.0 Hz, 1H), 7.90−7.87 (m, 1H), 7.62 (d, *J* = 8.5 Hz, 1H), 7.52−7.47 (m, 2H), 7.41−7.37 (m, 1H), 7.22 (s, 1H), 3.15 (t, *J* = 7.0 Hz, 2H), 2.77 (t, *J* = 7.0 Hz, 2H), 1.51 (s, 9H). ^{13}C NMR (101 MHz, DMSO-d_6): δ 170.1, 168.9, 165.5, 157.5, 152.0, 143.1, 134.5, 129.6, 126.9, 125.2, 122.4, 122.3, 114.2, 111.3, 106.7, 85.3, 37.1, 28.3, 26.5. HRMS-ESI calcd $[M - H]^+$ 431.1099; found, 431.1095.

*N-(4-(Benzo[d]thiazol-2-yl)-3-hydroxyphenyl)-3-mercaptopropanamide (**5a**).* To a solution of 47 mg (0.11 mmol) of **3a** in 1 mL of DCM were added 1 mL of TFA and 0.5 mL of anisole. The mixture was left stirring for 1 h or until no starting material was observed on the TLC. After the deprotection was completed, the solvent was removed under reduced pressure. The residue was diluted with 4 mL of water, neutralized with $NaHCO_3$ 10%, and extracted four times with 5 mL of DCM. The organic phase was dried over anhydrous $MgSO_4$, filtered, and concentrated. Yellow solid, 82% yield. FT-IR (ATR, cm^{-1}): ν 3270; 2922; 2843; 1649; 1496. ^{1}H NMR (400 MHz, $CDCl_3$): δ 12.42 (s, 1H), 8.13−8.09 (m, 1H), 7.98 (d, *J* = 8.2 Hz, 1H), 7.90 (d, *J* = 9.1 Hz, 1H), 7.54−7.47 (m, 1H), 7.45−7.36 (m, 1H), 7.33 (dd, *J* = 8.7, 2.4 Hz, 1H), 7.06 (d, *J* = 8.5 Hz, 1H), 2.99−2.85 (m, 2H), 2.70 (t, *J* = 6.6 Hz, 2H), 1.74 (t, *J* = 8.4 Hz, 1H). ^{13}C NMR (101 MHz, DMSO-d_6): δ 169.6, 165.2, 152.7, 152.0, 135.0, 132.1, 126.9, 125.6, 124.6, 122.6, 122.6, 119.2, 118.6, 117.6, 40.7, 20.3. HRMS-ESI calcd $[M - H]^+$ 331.0575; found, 331.0569.

*N-(4-(Benzo[d]thiazol-2-yl)-3-hydroxyphenyl)-3-mercaptopropanamide (**5b**).* The compound was prepared in the same way as **5a**. Pale-green solid, 99% yield. FT-IR (ATR, cm^{-1}): ν 3312; 1663; 1594; 1199; 1125; 971. ^{1}H NMR (400 MHz, $CDCl_3$): δ 7.99−7.90 (m, 1H), 7.92−7.83 (m, 1H), 7.67−7.58 (m, 1H), 7.54−7.43 (m, 1H), 7.44−7.33 (m, 1H), 7.34 (s, 1H), 7.23 (s, 2H), 2.97−2.84 (m, 2H), 2.71 (t, *J* = 6.6 Hz, 2H), 1.73 (t, *J* = 8.5 Hz, 1H). ^{13}C NMR (101 MHz, DMSO-d_6): δ 170.4, 152.0, 143.3, 134.5, 129.6, 126.9, 125.2, 122.4, 122.3, 114.1, 111.3, 106.8, 40.9, 20.1. HRMS-ESI calcd $[M - H]^+$ 331.0575; found, 331.0569.

Preparation of the Films. The solutions of **3a** and **3b** in different solvents were prepared to obtain spin-coated thin films with comparable absorption. The concentration of **3a** in DMF was equal to 30 mg/mL, while in the rest of the solvents, it was equal to 10 mg/mL. The solution of **3b** in DMF contained 19 mg/mL. The solutions were heated and stirred overnight. Given the low boiling point of ACN and chloroform, these solutions were heated at 50 °C, while DMF and toluene solutions were heated at 80 °C. Quartz substrates were cleaned in an ultrasonic bath, first with acetone and then with isopropanol, followed by an oxygen plasma treatment. Then, substrates and solutions were transferred into a glovebox, where the solutions were spin-coated on the substrates at 3000 rpm for 30 s. After spin coating, the samples for thermal annealing were placed on a hotplate at the corresponding temperature for 20 min.

UV−Vis and Fluorescence Spectroscopy. All solvents for absorption and fluorescence spectroscopy measurements

https://doi.org/10.1021/acs.jpcc.3c04543
J. Phys. Chem. C 2023, 127, 17624−17636

Scheme 1. Synthetic Pathway to Obtain the ESIPT Dyes with a Thiol Handle in Positions 4 (para) or 5 (meta) Relative to the Hydroxyl Group[a]

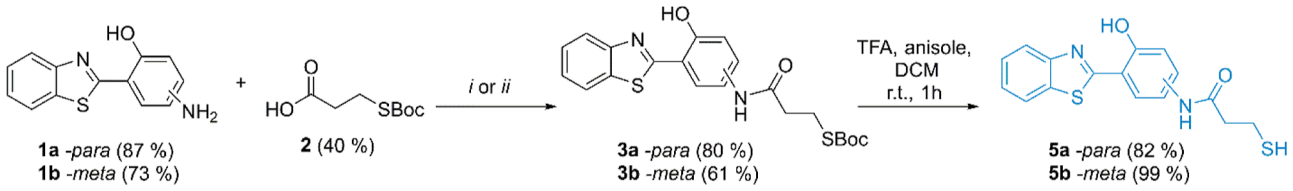

[a]For the coupling of **1a,** method *i* was employed (DCC, DMAP, 48 h in dry DCM). For dye **1b,** method *ii* was employed (DCC, HOBt, 48 h in dry DCM). A detailed description of the optimization conditions can be found in the Supporting Information.

were of HPLC grade, purchased from Chempur or Sigma-Aldrich. Absorption spectra in the UV−vis range were performed in a double beam UV−vis−NIR spectrometer Varian Inc. Carry 5000 in the range 200−800 nm with an optical path of 1 cm. All solutions and thin film samples were freshly made and measured right after. The FL measurements for the same solutions and thin films were conducted in the FLS980 spectrofluorometer, Edinburgh Instruments (UK) with a Xe lamp as an excitation source and an R-928 photomultiplier detector. The QYs were recorded by the absolute method employing an integrating sphere (Edinburgh Instruments with a BENFLEC interior coating) coupled to the equipment. In the case of thin films, the absorbed and emitted spectra were recorded when the samples were illuminated directly and indirectly, to consider both in the QY calculation.

Computational Methods. Density functional theory (DFT) calculations have been used to understand the reactivity of the HBT dyes. The ground state geometry of enol forms of **1a** and **1b** was calculated using the ωB97XD[34] functional with 6-311G(d,p) basis set as implemented in Gaussian 16, Revision C.01.[35] An integral equation formalism variant of the polarizable continuum model (IEFPCM)[36,37] was used to emulate the dichloromethane solvent effect. The Fukui index, HELP, and HELV values were calculated with the Multiwfn[38] package. All molecular images were made with ChimeraX.[39,40]

DFT and its time-dependent version (TD-DFT) calculations have been used to investigate the photophysical properties of the dyes. The ground state (GS) geometry of **5a** and **5b** was optimized using density functional B3LYP.[41] No imaginary frequencies were found. The 6-311G(d,p) basis set was employed in the description of the atomic electrons, as implemented in Gaussian 16, Revision C.01.[35] IEFPCM[36,37] was used to emulate the dichloromethane solvent effect. The electronically excited-state geometry was optimized using TD-DFT formalism using the same functional and basis set of the GS.

RESULTS AND DISCUSSION

The modifications on the amino-HBT core carried out in this study were planned considering two aspects: first, it should be kept as simple as possible, and second, to leave the possibility to further reactions. In general, molecules are designed as "closed structures". In other words, without the presence of groups, which can still react without directly affecting the fluorescent properties of the dye. These kinds of groups are of great importance to generate covalent bonds with a substrate, like proteins or polymers, or when it is necessary to achieve high control of the number of ligands. As outlined in Scheme 1, two amino-HBT derivatives bearing a short arm holding a thiol group as a chemical handle linked to positions 4 (para) or 5 (meta) relative to the hydroxyl group (**5a** and **5b**, respectively) were prepared.

The amino-HBT derivatives were synthesized as previously described in the literature.[12,32] To introduce the thiol function, we employed 3-mercaptopropionic acid (MPA). Due to the requirement to protect the MPA with *tert*-butyloxycarbonyl (Boc), mild conditions were applied. The activation of the carboxylic acid to the respective acyl chloride could not be used since it results in in situ HCl formation, which would promote the removal of the sulfur protective group.[42] Interestingly, the two isomers showed different behaviors at the coupling stage. For the HBT derivative **1a**, the classic coupling agents DCC/DMAP proved to be adequate.[43,44] The desired amide product **3a** was obtained with an 80% yield. It is well known that when both amino and hydroxyl groups are present in a molecule, a mixture between the amide and ester products can occur. However, as expected, in the absence of a base, only small amounts of the respective ester isomer (**4a**) were isolated (see Table S1).

For the meta-amino-HBT **1b,** the systems employing DCC/DMAP did not perform well, and **3b** was obtained in poor yields (entries 1, 2, and 3, Table S2). Despite employing various experimental conditions with DCC/DMAP as coupling agents, in none of them, it was possible to identify the formation of the ester **4b** (Table S2), and a large portion of the starting material was recovered in the end. Since in **1b**, the amino group is opposite to the strong EWG benzothiazole ring, we expected that the push−pull effect would remove electronic density from the nitrogen, thereby leaving it less nucleophilic than in isomer **1a**. To confirm this, the Fukui nucleophilicity index (f^-), high electron localization function domain (HELP),[45] and volume (HELV) indexes for both compounds were calculated. As expected, the Fukui index for the amino group of **1b** was smaller when compared to para isomer **1a**. For isomer **1a**, the value of the condensed f^- is equal to 0.14 for the nitrogen of the amine group. In molecule **1b**, the condensed f^- is equal to 0.11 for the nitrogen. A similar tendency was observed for the HELP scores (Figure S1). This implies a relatively smaller electron density at the nitrogen of the amino group in **1b** when compared with **1a**. Since both amino and hydroxyl groups are EDGs, in the case of the para molecule, there is a compensation between the donation of electrons of the N by the O on the opposite side, which does not apply for **1b**. These electronic effects can also be observed in the HOMO distribution for both compounds (Figures S2 and S3). For **1a**, the HOMO was localized at the phenolic ring, while for **1b**, it was distributed all over the molecule, clearly showing a relationship between the electronic distribution of the molecule and the position of the amino group. The lesser

https://doi.org/10.1021/acs.jpcc.3c04543
J. Phys. Chem. C 2023, 127, 17624−17636

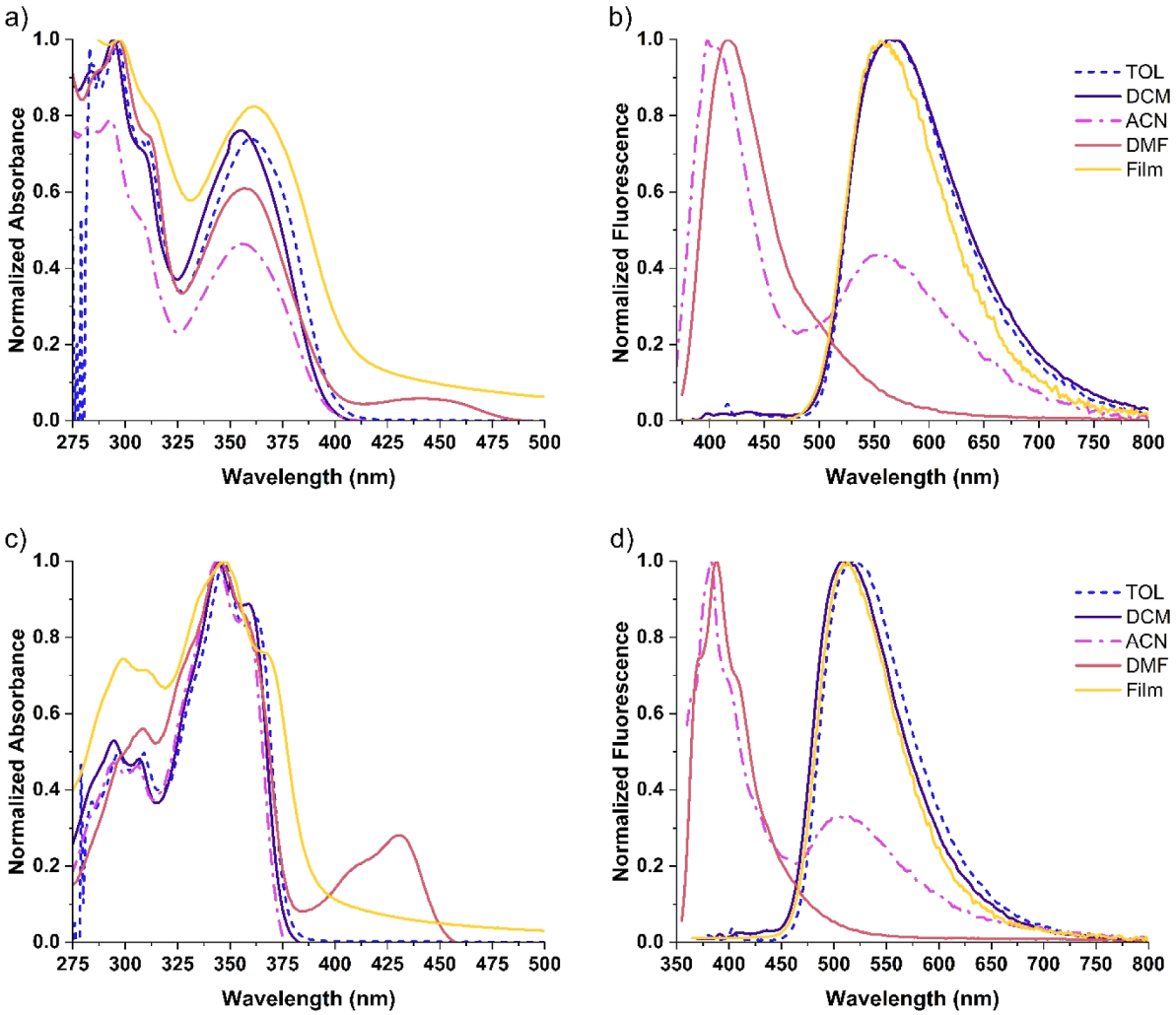

Figure 1. Normalized UV−vis and FL spectra for compounds **5a** (graphs a and b) and **5b** (graphs c and d) in TOL, DCM, ACN, and DMF and in solid state (Film). [**5a**] = 25 μM and [**5b**] = 2.5 μM. Films spin-coated on quartz from the DMF solution of the respective Boc-protected compounds.

Table 1. Summary of UV−Vis and FL Data for Compounds 5a and 5b in Solution and Solid States (Film)

compound	solvent	λ_{abs} (nm)	$\varepsilon \times 10^4$ (L mol^{-1}cm^{-1})	Eλ_{ems} (nm)	ΔST_{enol} (cm^{-1})	Kλ_{ems} (nm)	ΔST_{keto} (cm^{-1})	Dλ_{ems} (nm)	ΔST_{depr} (cm^{-1})	QY[c] (%)
5a	TOL	360	1.2			565	10,079			1.0
	DCM	355	1.2			565	10,469			<1.0
	ACN	355	1.0	400	3169	560	10,312			<1.0
	DMF[a]	358/430	1.0/0.1	420	4123			502	3336	14.4
	film[b]	361				560	9767			12.4
5b	TOL	347	4.8			520	9588			3.0
	DCM	345	4.4			510	9378			1.0
	ACN	343	2.0	385	3180	500	9155			<1.0
	DMF[a]	347/430	1.8 /0.4	390	3177			462	1611	19.2
	film[b]	347				510	9211			16.9

[a]Measurements in DMF solutions were conducted at both wavelengths to maintain the comparison with other solvents. [b]Measurements of as-deposited films were done using the respective Boc-protected compound from the DMF solution. [c]Absolute QYs were measured using an integrating sphere with an estimated error of 1%.

reactivity of **1b** might also be one of the reasons why most of the very few amino-HBT derivatives described in the literature are synthesized with para substitutions only.[46]

Interestingly, when HOBt was used as an additive instead of DMAP, the scenario changed. Although the OBt active ester is less reactive than the *O*-acyl urea, the efficacy increased and the formation of **3b** was improved (entries 4, 5, and 6, Table S2). This enhancement is probably connected to the fact that the OBt ester is free of rearrangement to the inactive *N*-acylurea.[47] Moreover, the OBt ester can also assist the approach of the amino-HBT through hydrogen bonds.[48] The best conditions were obtained when a slight excess of the coupling agents was

https://doi.org/10.1021/acs.jpcc.3c04543
J. Phys. Chem. C 2023, 127, 17624−17636

employed and the desired amide **3b** was obtained with 61% yield. The dependence of the reactivity with the respective coupling additive (DMAP or HOBt) highlights the differences in the push−pull balance for the para and meta isomers as predicted by the calculations. While for compound **1a**, the para position between the hydroxy and amino groups compensates the EWG effects of the benzothiazole ring, the same is not observed for **1b**, where the amino group was noticeably less nucleophilic. These effects were confirmed both experimentally and theoretically. The different push−pull balances were also expected to affect the surrounding environment of the molecules and the physicochemical properties of the obtained material. The deprotections of **3a** and **3b** to the free thiols **5a** and **5b** were done as described in Scheme 1 with good yields, 82 and 99%, respectively. All new compounds, including the Boc-protected intermediates, were fully characterized, and their NMR spectra are shown in the Supporting Information.

PHOTOPHYSICAL PROPERTIES

To investigate the photophysical properties of the compounds in different environments, UV−vis and FL measurements were performed in dichloromethane (DCM), toluene (TOL), acetonitrile (ACN), and *N*,*N*-dimethylformamide (DMF) as well in the solid state, through the preparation of spin-coated films. The UV−vis and FL emission spectra for compounds **5a** and **5b** are shown in Figure 1, and the relevant spectroscopic data is summarized in Table 1. The respective Boc-protected compounds **3a** and **3b** showed identical spectroscopic profiles to the final materials. For comparison, the absorption and emission spectra are displayed in Figure S4, and the summarized photophysical data can be found in Table S3, and the same following discussion can be rationalized for these compounds.

As can be seen in Figure 1, compounds **5a** and **5b**, despite their structural similarity, show remarkably different behaviors of the UV−vis spectra. First, the significantly higher molar absorptivity coefficient (ε) in the case of **5b** implies the use of a lower concentration range for this compound. Second, the presence of two bands in the UV−vis spectra of **5a** was in contrast with the single band with the shoulder of **5b**. The longer wavelength absorption maximum for **5a** solution in toluene was slightly redshifted (360 nm) with respect to DCM, ACN, or DMF (∼355 nm) solutions. On the contrary, no significant shifts were observed for **5b** samples, for which the maximum remained around 350 nm. Although the absorption bands were broader, the maximum absorption wavelength remained the same in the case of thin films, with the absence of additional bands. A decrease of ε values was observed for both compounds when the solvent polarity increased. The absorption coefficient was almost four times larger for **5b** than for **5a** in toluene and DCM and two times larger in ACN and DMF. In both cases, the absorption maxima can be assigned to $\pi \rightarrow \pi^*$ transitions, which are typical for polyaromatic dyes.[49,50]

When comparing the $\pi \rightarrow \pi^*$ transition wavelengths of **5a** and **5b** with the respective amino-HBT parent compounds (**1a** λ_{abs} = 384 nm and **1b** λ_{abs} = 351 nm),[12] it is possible to notice that the introduction of the amide bond produced a blue shift in both cases, possibly due to EWG effects of the carbonyl group.[43] However, the shifts were bigger for **5a** (∼30 nm) than for **5b** (∼5 nm) in all solvents, most probably because in **5b**, the carbonyl group is opposite to a stronger EWG which counterbalances the push−pull effect caused by the benzothiazole ring.

In the FL spectra of TOL and DCM, both **5a** and **5b** showed a single broad band around 565 nm and 515 nm, respectively, which can be attributed to the K* emission. Only a negligible E* emission was observed, which indicates an efficient ESIPT mechanism for these solvents. As a result, large Stokes shifts were observed for **5a** in toluene (10,079 cm^{-1}) and in DCM (10,469 cm^{-1}), and also for compound **5b**, equal to 9588 and 9378 cm^{-1} in TOL and DCM, respectively. Comparing emission wavelengths of K* of **5a** and **5b** to the K* emission of the respective starting material **1a** (606 nm) and **1b** (500 nm),[12] the opposite spectral shifts were noticed. For para isomer **5a**, a blue shift of ∼40 nm was observed, while meta isomer **5b** revealed a red shift of ∼15 nm.

When the solvents were changed to the polar aprotic ACN and DMF, two distinct tendencies were observed. In ACN, both dyes displayed dual E*/K* emissions. In contrast, in DMF, only the enol emission was evidenced for both compounds, which means that the ESIPT process was completely frustrated, resulting in much smaller Stokes shifts, equal to 4123 and 3177 cm^{-1} for **5a** and **5b**, respectively. Moreover, an additional absorption band around 430 nm was noticed for both compounds in DMF, which can be assigned to the deprotonation of the hydroxyl group (Scheme S1). Analogical behavior of the deprotonated conjugate base (D) has been reported for other HBT derivatives with triple E*/D*/K* emission, which was rationally employed for white light emission applications.[17,51] Although the films were prepared from DMF solutions due to the better solubility in this solvent, they showed FL spectra similar to the TOL and DCM solutions, namely, with only one band present and matching the K* emission.

With respect to the QY, both compounds showed to be weak emitters in solution, which is a common feature of ESIPT molecules resulting from the large amplitude molecular motions. In particular, the mutual rotation of phenol and benzothiazole rings promotes non-radiative deactivations.[52] It is worth noting that in DMF, the QY increased to 14.4 and 19.2% for **5a** and **5b**, respectively. Since the keto emission was not present in DMF, the conical intersection with the GS, which can lead to deactivation of the ESIPT process, was no longer affecting the FL, resulting in higher QY values in this solvent.[51,52] Higher QY values were found for **5b** than for **5a** in both DMF solution and thin film samples, implying that the presence of the amide group opposite to the strong EWG benzothiazole moiety results in lowering of radiative losses regardless of the emissive mechanism. For the films of both compounds, it is worth mentioning that a strong increase in the QY was observed in comparison to the solutions of TOL or DCM. This indicates the presence of a solid-state fluorescence enhancement, due to the rigidification of the environment and the steric restriction of large-amplitude molecular motions in the films.

COMPUTATIONAL STUDIES

To better understand the opposite shifts observed in the FL spectra, we employed DFT and TD-DFT methodologies to calculate the HOMO/LUMO for both final compounds. The computational molecular modeling was performed in the ground and in the excited state, considering DCM as the solvent (Table S4, where only the K* emission was observed) and in DMF (Table S5, where E* and D* emissions were

https://doi.org/10.1021/acs.jpcc.3c04543
J. Phys. Chem. C 2023, 127, 17624−17636

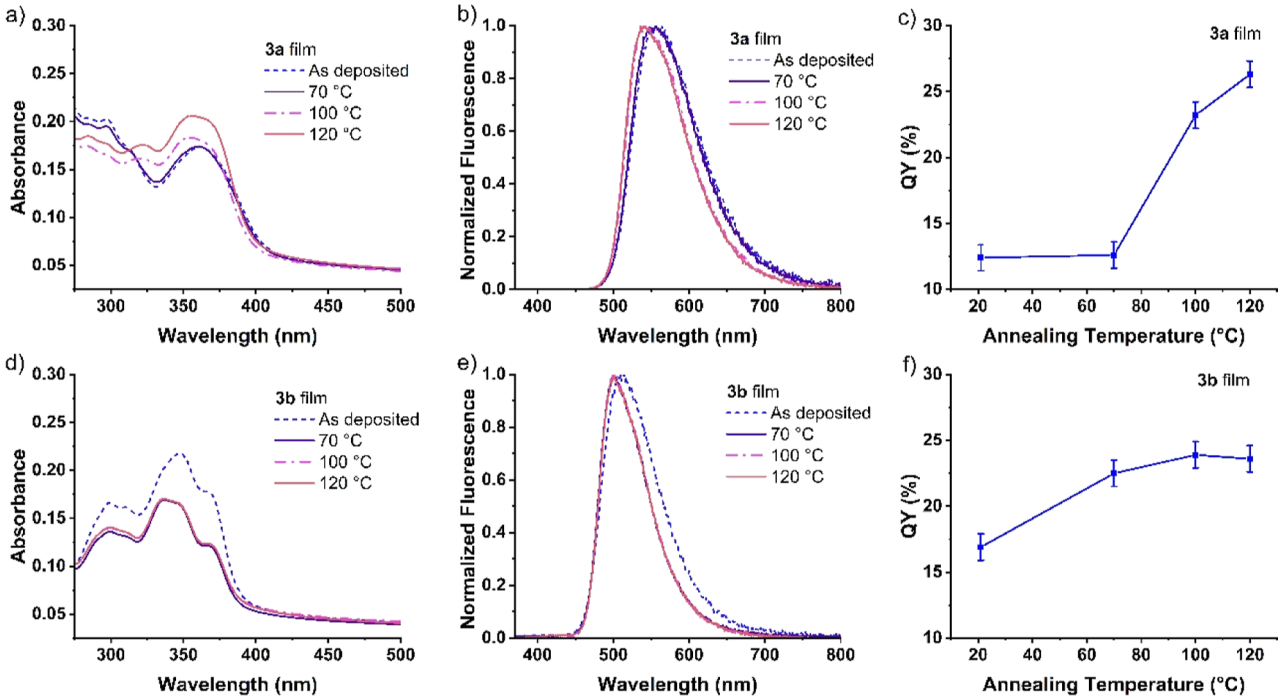

Figure 2. (a) Absorbance, (b) fluorescence, and (c) QY for **3a** films and (d) absorbance, (e) fluorescence, and (f) QY for **3b** films with respect to the annealing temperature. All films were spin-coated from DMF solutions.

present). In DCM, the optimized GS geometries for the enol tautomer of **5a** (Figure S5) and **5b** (Figure S6) showed a coplanar geometry between the benzothiazole moiety and the phenyl ring, which remains unchanged after electronic excitation. This geometry allows the full π-conjugation between these two units and, consequently, electronic delocalization along the π-backbone. Furthermore, the π-conjugation extends over to the amide group in the GS for these molecules. Although this extension of π-conjugation was present in the LUMO of **5b**, which contributes to a redshifted emission with respect to its amine analogue **1b**, this was not true for the LUMO of **5a**. For dye **5a**, the π-conjugation was present only at the HBT moiety, resulting in a blue-shifted ESIPT emission when compared to its amino analogue **1a**.[53]

The calculated excitation (absorption) wavelengths, for the $S_0 \rightarrow S_1$ transition, for **5a** and **5b** were equal to 370.9 and 346.9 nm, respectively. These values were in close agreement with the experimental data obtained for the DCM solutions. For isomer **5a**, the calculated absorption wavelength was 4.5% greater than the experimental peak at 355 nm, and for **5b**, the excitation wavelength was only 0.5% greater than the experimental value of 345 nm. The orbitals involved in the $S_0 \rightarrow S_1$ transition for the enol tautomer of **5a** were HOMO and LUMO. The oscillator strength (f) for this transition was equal to 0.3127, indicating an allowed transition between these Frontier molecular orbitals (FMO). The same type of HOMO to LUMO electronic excitation was also present in **5b**, where f was equal to 1.0009. Due to the symmetry of the FMO of both molecules, it was classified as a $\pi \rightarrow \pi^*$ excitation, which is in agreement with the experimental results. The greater value of f for **5b** was in agreement with the experimental data since **5b** showed higher ε values than **5a**. The broad band between 275 and 325 nm could be explained by the transition between the internal orbitals and the unoccupied FMO.

An additional band around 430 nm was observed for DMF solutions of both compounds. This band corresponds to the $S_0 \rightarrow S_1$ transition of the deprotonated (D) species. The f values of the D species for dyes **5a** and **5b** were 0.4520 and 0.5283, respectively. Similar to DCM solutions, the f values of the $S_0 \rightarrow S_1$ transitions in DMF were higher for **5b** than for **5a**. This behavior also follows the results of experimental measurements.

As a result of the S_1 state optimization in DCM by TD-DFT, the HOMO energy increased, followed by a decrease in the LUMO energy of the enol form. This change in the HOMO/LUMO energy upon excitation led to a decrease in the frontier orbital gap of 3.843 eV in the GS to 3.333 eV in the S_1 state for molecule **5a**. This change was even more pronounced for molecule **5b**, for which the energy gap between the FMO decreased from 4.047 eV in the GS to 3.515 eV in the E S_1 state.

According to Kasha's rule,[54] the emissive properties of molecules are mostly determined by the lowest-lying singlet excited state, and higher electronic excited states are not directly involved in photon emission. Therefore, these states will not be considered here. The calculated emission wavelength of the $S_0 \rightarrow S_1$ transition of the keto tautomer in DCM was equal to 516.8 and 468.7 nm for **5a** and **5b**, respectively, which is in agreement with the experimental results. In DMF, the calculated emission energies of the $S_0 \rightarrow S_1$ transition of the enol tautomer of **5a** and **5b** were 436.3 and 393.6 nm, respectively, which is also in good agreement with experimental data.

Temperature and Solvent Studies in Thin Films. Neat thin films were prepared by spin coating the new amide-HBT materials on quartz substrates for further characterization. As previously reported,[55−58] the side chain nature, length, and position in the molecule backbone influence the solubility, packing, and electronic properties of organic molecules in thin

https://doi.org/10.1021/acs.jpcc.3c04543
J. Phys. Chem. C 2023, 127, 17624−17636

Table 2. Photophysical Parameters for the 3a and 3b Films Annealed at Different Temperatures

molecule	T (°C)	λ_{abs} (nm)	Abs (a.u.)	λ_{FL} (nm)	FWHM (nm)	QY (%)	roughness Sq (nm)
3a		361	0.170	559	102	12.4	0.47
	70	361	0.170	555	98	12.6	0.98
	100	356	0.183	541	92	23.2	2.6
	120	356	0.206	541	92	26.3	4.7
3b		347	0.218	512	84	16.9	1.2
	70	337	0.170	501	72	22.5	5.1
	100	337	0.170	502	71	23.9	6.5
	120	337	0.170	501	70	23.6	6.6

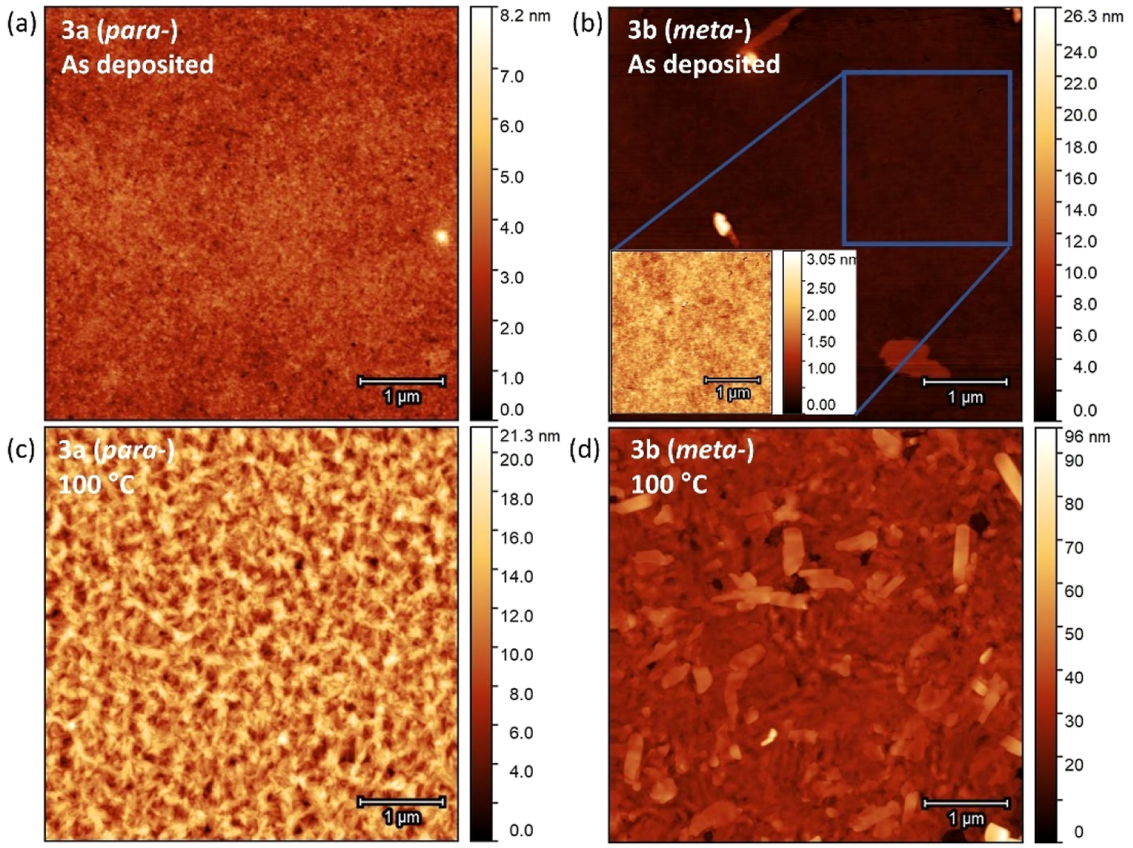

Figure 3. AFM images of (a) **3a** and (b) **3b** films as-deposited and (c) **3a** and (d) **3b** films annealed at 100 °C. Both materials were deposited from DMF solutions. The inset in (c) shows the image of a representative area of the homogeneous roughness of 3 μm × 3 μm. The rest of the images represent a sample area of 5 μm × 5 μm.

films. Therefore, based on the solution studies, we could expect to obtain different optical properties of para and meta molecules in thin films due to the non-identical push−pull effects in both isomers. Given the low solubility of the thiol material (**5a** and **5b**) in most common solvents, we focused our study on the Boc-protected molecules (**3a** and **3b**), which showed identical photophysical performance to the final thiol molecule in solution. In addition, the presence of the *tert*-butyl group is widely employed in the preparation of organic materials since it increases the processability by reducing intermolecular contact without drastically impacting the fluorescent properties.[59] Since both molecules presented good solubilities in DMF, this solvent was chosen for thin film studies. As previously commented, the absorption and emission spectra of thin films revealed similar features to the results of solution studies. The meta molecule **3b** presented a higher QY, a shorter maximum wavelength, and a narrower emission, which suggests a more planar molecular orientation, together with a closer intermolecular packing,[8,30,60,61] in comparison to the para isomer **3a**. It should be recalled that this is also in consonance with the calculated geometry of the molecules (Supporting Information).

Based on the results of differential scanning calorimetry (DSC) of **3a** (Figure S7), which showed a thermal transition between 80 and 100 °C, samples of the thin films annealed at 70, 100, and 120 °C were prepared. It is worth noting that the DSC spectrum of molecule **3b** did not show any sign of thermal transition. However, the same annealing temperatures were considered to analyze the effects of the same conditions on both molecules. Then, the film's absorption, emission, and morphology were measured and compared.

The absorbances of the thin films are shown in Figure 2a,d for para and meta dyes, respectively. The thin film of **3a** showed a broader maximum peak and an increase in the absorbance when it was annealed above 70 °C. The same broadening, together with an absorbance decrease, was

https://doi.org/10.1021/acs.jpcc.3c04543
J. Phys. Chem. C 2023, 127, 17624−17636

observed in thin films made from molecule **3b**, however, occurring at lower annealing temperatures. The different changes in the absorbance trend can be associated with the modified film morphology as will be discussed later with the results obtained from atomic force microscopy (AFM). Regarding the effect of thermal annealing on the FL, changes in the spectra were observed at the same temperatures as in the UV−vis absorption of both compounds. As shown in Figure 2b and in the parameters described in Table 2, annealing temperatures above 70 °C for molecule **3a** provided a 5 nm blue shift of the peak maximum as well as an ∼8 nm narrowing of the full width at half-maximum (FWHM) emitted spectra. A similar effect was observed for **3b** (Figure 2e); however, at a lower temperature, and, in addition, with a larger blue shift and more pronounced narrowing (10 and ∼13 nm, respectively). Those changes can be attributed to the effect of thermal annealing on the molecular packing and orientational order of molecules in the film.[62−64] It must be noted that slit widths for the emission spectra measurement of each sample were different in order to avoid detector saturation. Therefore, spectra in Figure 2b,e are normalized. The thermal energy provided to the material may contribute to the molecular rearrangement, yielding more structured surfaces of the spin-coated films. These topographical changes result from the redistribution of the molecules and therefore the modification of the intermolecular interactions. This fact led us to analyze the effect of thermal annealing on the films QY. As demonstrated in Figure 2c,f, overcoming the same temperature threshold that induced changes in the absorptive and fluorescent properties for each molecule, also comprised an enhancement in the QY of thin films. In particular, the QY of **3a** was abruptly enhanced when the annealing temperature reached 100 °C, increasing by about 85% with respect to a 70 °C annealing. However, the meta isomer **3b** showed a more linear QY enhancement, being approximately 25% larger when the film was annealed at 70 °C compared to the as-deposited film. The different trend on the QY enhancement between the two molecules supported the observations made during the spectroscopic characterization of the non-annealed films, which indicated that **3b** was already more planarly oriented and closer packed than **3a**. However, higher structural molecular order and larger suppression of the vibronic relaxation from the excited state were achieved for thin films of **3b** after thermal annealing, provided by the more pronounced narrowing of the FWHM emitted spectrum.[61,65] Such narrowing also indicates that the crystallinity degree in the final films may vary between both isomers.

To further explore the possible contributions to the photophysical properties found in the annealed films, their surface morphology was studied. Figure 3 depicts the surface morphology obtained from AFM of **3a** and **3b** samples as-deposited and annealed at 100 °C. Both non-annealed samples present similar morphologies if the anecdotic defects are excluded (the inset in Figure 3c shows a representative sample area). Moreover, both films showed an evident change in their surface morphology after thermal treatment, although they are clearly different. The annealed thin film of **3a** (Figure 3c) showed an amorphous morphology with larger area domains than the respective as-deposited film (Figure 3a). On the other hand, the annealed thin films of **3b** exhibited more crystalline and oriented features (Figure 3d). As a result of such morphologies, the surface roughness, whose values are included in Table 2, increased when thermal annealing was applied. For **3a**, the homogeneous, rougher surface acts as the textured interface and is probably one of the reasons why the absorption of the film increases.[66] In fact, the rougher the surface of the annealed samples for this material, the higher the absorption observed in the thin films. The resulting morphology for **3a** seems to contribute to a higher FL QY of thin films when the annealing was performed above the temperature threshold, since lower interdomain quenching and better light outcoupling after photon generation are expected. In contrast, the increased roughness of the annealed films of **3b** was produced by a non-uniform distribution of crystallites and some pinholes created on the film surface. Therefore, in this case, such pinhole generation may cause the absorption of the film to decrease after annealing, as previously described. However, the formed crystallites imply a higher molecule order in their structure, which is in accordance with the previously discussed narrowing of the FWHM emission. The generation of a crystalline morphology, together with the considerable narrowing of the emitted spectra, suggests that the application of thermal postprocessing techniques may be suitable for the induction and/or enhancement of amplified spontaneous emission in ESIPT and related lasing applications.[18,67,68] It is important to note that Figure 3 shows materials with the same post-treatment (100 °C), but in case of molecule **3b**, the changes were observed at a lower temperature. Figure S8 presents the AFM images of samples annealed at 70 and 120 °C, which also showed a morphological evolution in accordance with the spectroscopy results.

Given the different FL results produced by the thermal annealing of the films and their clear connection to the film morphology, the effect of the solvent employed for thin film fabrication was studied. Solvent properties, including volatility and specific solvent−solute interactions, are known to have a significant impact on the morphology of solution-processed films.[69−71] While molecule **3a** was easily dissolved in many different solvents, molecule **3b** was less soluble to obtain an acceptable concentration to produce continuous thin films by spin coating. Therefore, only **3a** was employed for such a study, and it was deposited from four different solvents: DMF, ACN, chloroform, and TOL. After the depositions, all films were annealed at 100 °C since it was previously proven to provide better QY and define the final film morphology. Figure S9 shows the normalized absorbance and FL spectra obtained from films annealed at 100 °C, demonstrating that the solvent did not considerably affect the spectral properties of **3a**. However, the QY (Table 3) showed higher efficiency for the films deposited from chloroform and TOL compared to those obtained from DMF and ACN. To analyze the possible causes for different values of QY the films were studied by AFM. The AFM images showed two different types of morphology, matching the two groups of solvents regarding QY efficiencies. As demonstrated in Figure 4, chloroform and TOL samples showed a lamellar-like morphology, which implies a higher

Table 3. Photophysical Parameters of 3a Films Fabricated from Solutions in Different Solvents Annealed at 100 °C

molecule	solvent	λ_{abs} (nm)	λ_{FL} (nm)	FWHM (nm)	QY (%)
3a	DMF	356	541	92	23.2
	ACN	356	545	92	20.8
	chloroform	356	540	90	31.0
	toluene	355	538	89	26.4

https://doi.org/10.1021/acs.jpcc.3c04543
J. Phys. Chem. C 2023, 127, 17624−17636

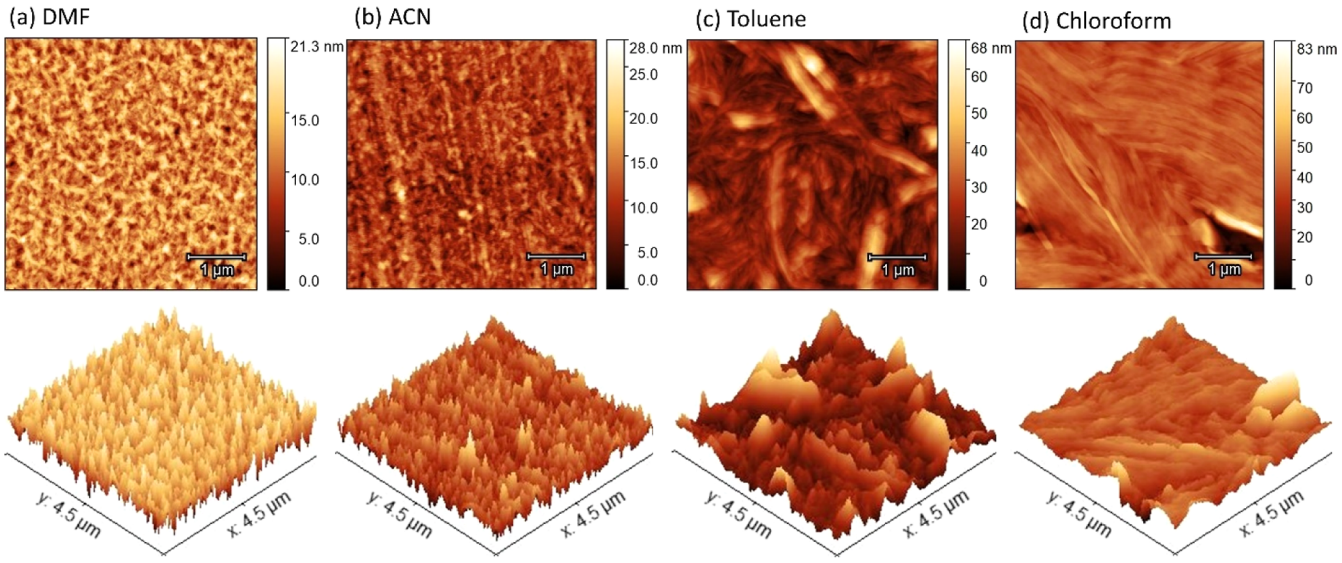

Figure 4. AFM images of **3a** films fabricated from solutions in different solvents: (a) DMF, (b) ACN, (c) toluene, and (d) chloroform annealed at 100 °C.

degree of orientation in the continuous domains generated. On the contrary, DMF and ACN samples showed less anisotropic morphology with a topology showing more random interconnections. Those results are in accordance with the fact that the induction of more compact and directional molecular packing provides a higher QY. Therefore, chloroform can be considered as the most suitable solvent for thin films of studied dyes, as manifested by FL emission with a QY of 31%. This result evidences that the combination of mild thermal annealing and the correct solvent selection can provide an enhancement of at least 150% on the QY of the fabricated thin films.

Finally, to confirm that the effect of the thermal annealing acted independently of the solvent employed, the absorption, FL, and QY of the samples as-deposited and annealed at 100 °C were compared. Table S6 shows an analogous behavior after annealing to the one described for samples made from DMF. The FL of all the thin films is ascribed to the K* emission independently of the solvent employed for their fabrication. This result confirms that using DMF as the solvent for thin film deposition does not modify the molecule when it is deposited, even if DMF is able to deprotonate the material in the solution. In addition, a higher QY enhancement was obtained for the annealed samples with more lamellar-like morphology, i.e., TOL and chloroform. These results demonstrate that ESIPT performance in thin films can be optimized by properly selecting the solvent and the postprocessing parameters.

CONCLUSIONS

The straightforward synthesis of new ESIPT derivatives and their molecular and spectroscopic properties, focusing on the effects of the push−pull system of the para and meta isomers, was reported. In the starting material, experiments and theoretical calculations reinforced that the push−pull balance strongly determines the amino group nucleophilicity. In addition, we were able to obtain and characterize a much less explored meta derivative. In the newly synthesized molecules, the photophysical analysis supported by computational studies revealed that the introduced amide group responds differently to the EWG of the benzothiazole moiety due to different push−pull balances in the isomers. For both compounds, **5a** and **5b**, a dependence of the solvent polarity on the E*/K* emission rate was observed. Spectroscopic and morphological studies of spin-coated neat films presented narrower and more efficient emissions for compound **3b**, provided by more favorable intermolecular interactions between the molecules when compared to compound **3a**. Such interactions could be further enhanced by tuning the molecular arrangement through the thermal annealing of thin films and the solvent selection of the solution employed, as shown by the AFM studies. Moreover, it was demonstrated that the FWHM was narrowed and the QY of the films could be increased up to 150% by a simple combination of thermal treatment and solvent selection. These results open an optimization path and a new field of study for ESIPT materials and, more particularly, HBT molecules when these materials are intended to be applied in thin film technologies, such as in organic light emitting devices, optical lasers, or down-conversion materials.

ASSOCIATED CONTENT

Supporting Information

The Supporting Information is available free of charge at https://pubs.acs.org/doi/10.1021/acs.jpcc.3c04543.

Additional discussions about theoretical calculations, experimental procedures and results, and spectroscopic data for ^{1}H NMR and ^{13}C NMR of all compounds synthesized (PDF)

AUTHOR INFORMATION

Corresponding Authors

Franciela Arenhart Soares − *International Centre for Research on Innovative Biobased Materials (ICRI-BioM)—International Research Agenda, Lodz University of Technology, 90-924 Lodz, Poland;* orcid.org/0000-0002-6624-9533; Email: franciela.arenhart-soares@p.lodz.pl

Piotr Ślęczkowski − *International Centre for Research on Innovative Biobased Materials (ICRI-BioM)—International Research Agenda, Lodz University of Technology, 90-924*

https://doi.org/10.1021/acs.jpcc.3c04543
J. Phys. Chem. C 2023, 127, 17624−17636

Lodz, Poland; orcid.org/0000-0002-9257-6116; Email: piotr.sleczkowski@p.lodz.pl

Authors

Guillermo Martinez-Denegri − *International Centre for Research on Innovative Biobased Materials (ICRI-BioM)—International Research Agenda, Lodz University of Technology, 90-924 Lodz, Poland*

Luis Andre Baptista − *Max Planck Institute for Polymer Research, 55128 Mainz, Germany;* orcid.org/0000-0002-1419-6070

Alexander Steinbüchel − *International Centre for Research on Innovative Biobased Materials (ICRI-BioM)—International Research Agenda, Lodz University of Technology, 90-924 Lodz, Poland*

Complete contact information is available at: https://pubs.acs.org/10.1021/acs.jpcc.3c04543

Author Contributions

The manuscript was written through contributions of all authors. All authors have given approval to the final version of the manuscript.

Notes

The authors declare no competing financial interest.

■ ACKNOWLEDGMENTS

The authors acknowledge the Foundation for Polish Science for the financing for the researchers (MAB PLUS/2019/11) and the National Science Centre, Poland (MINIATURA 5 grant, 2021/05/X/ST4/00572). The authors thank Robinson Cortes-Huerto for the critical reading of the manuscript. The authors acknowledge Marcin Kozanecki for helpful guidance in DSC studies and to Gabriela Wiosna-Sałyga for fruitful discussions.

■ REFERENCES

(1) Zhou, P.; Han, K. Unraveling the Detailed Mechanism of Excited-State Proton Transfer. *Acc. Chem. Res.* **2018**, *51*, 1681−1690.

(2) Cordeiro Dantas, W. F.; Duarte, L. G. T. A.; Rodembusch, F. S.; Poppi, R. J.; Zambon Atvars, T. D. Evaluation of the Acidic Strengths on Electronic Ground and Excited States of Proton Transfer Dye Using Excitation-Emission Fluorescence Matrix (EEM) and Multivariate Curve Resolution with Alternating Least Squares (MCR-ALS). *Methods Appl. Fluoresc.* **2020**, *8*, 045006.

(3) Hrobárik, P.; Hrobáriková, V.; Sigmundová, I.; Zahradník, P.; Fakis, M.; Polyzos, I.; Persephonis, P. Benzothiazoles with Tunable Electron-Withdrawing Strength and Reverse Polarity: A Route to Triphenylamine-Based Chromophores with Enhanced Two-Photon Absorption. *J. Org. Chem.* **2011**, *76*, 8726−8736.

(4) Zeng, G.; Liang, Z.; Jiang, X.; Quan, T.; Chen, T. An ESIPT-Dependent AIE Fluorophore Based on HBT Derivative: Substituent Positional Impact on Aggregated Luminescence and Its Application for Hydrogen Peroxide Detection. *Chem.—Eur. J.* **2022**, *28*, No. e202103241.

(5) Belmonte-Vázquez, J. L.; Amador-Sánchez, Y. A.; Rodríguez-Cortés, L. A.; Rodríguez-Molina, B. Dual-State Emission (DSE) in Organic Fluorophores: Design and Applications. *Chem. Mater.* **2021**, *33*, 7160−7184.

(6) Cai, M.; Gao, Z.; Zhou, X.; Wang, X.; Chen, S.; Zhao, Y.; Qian, Y.; Shi, N.; Mi, B.; Xie, L.; et al. A Small Change in Molecular Structure, a Big Difference in the AIEE Mechanism. *Phys. Chem. Chem. Phys.* **2012**, *14*, 5289−5296.

(7) Salla, C. A. M.; Teixeira dos Santos, J.; Farias, G.; Bortoluzi, A. J.; Curcio, S. F.; Cazati, T.; Izsák, R.; Neese, F.; de Souza, B.; Bechtold, I. H. New Boron(III) Blue Emitters for All-Solution Processed OLEDs: Molecular Design Assisted by Theoretical Modeling. *Eur. J. Inorg. Chem.* **2019**, 2247−2257.

(8) Mutai, T.; Sawatani, H.; Shida, T.; Shono, H.; Araki, K. Tuning of Excited-State Intramolecular Proton Transfer (ESIPT) Fluorescence of Imidazo[1,2-a]Pyridine in Rigid Matrices by Substitution Effect. *J. Org. Chem.* **2013**, *78*, 2482−2489.

(9) Pariat, T.; Munch, M.; Durko-Maciag, M.; Mysliwiec, J.; Retailleau, P.; Vérité, P. M.; Jacquemin, D.; Massue, J.; Ulrich, G. Impact of Heteroatom Substitution on Dual-State Emissive Rigidified 2-(2'-Hydroxyphenyl)Benzazole Dyes: Towards Ultra-Bright ESIPT Fluorophores. *Chem.−Eur. J.* **2021**, *27*, 3483−3495.

(10) Shukla, A.; Mai, V. T. N.; Divya, V. V.; Suresh, C. H.; Paul, M.; Karunakaran, V.; McGregor, S. K. M.; Allison, I.; Narayanan Unni, K. N.; Ajayaghosh, A.; et al. Amplified Spontaneous Emission from Zwitterionic Excited-State Intramolecular Proton Transfer. *J. Am. Chem. Soc.* **2022**, *144*, 13499−13510.

(11) Stoerkler, T.; Pariat, T.; Laurent, A. D.; Jacquemin, D.; Ulrich, G.; Massue, J. Sterically Hindered 2-(2'-Hydroxyphenyl)Benzoxazole (HBO) Emitters: Synthesis, Spectroscopic Studies, and Theoretical Calculations. *Eur. J. Org Chem.* **2022**, No. e202200661.

(12) Rodembusch, F. S.; Leusin, F. P.; Campo, L. F.; Stefani, V. Excited State Intramolecular Proton Transfer in Amino 2-(2′-Hydroxyphenyl)Benzazole Derivatives: Effects of the Solvent and the Amino Group Position. *J. Lumin.* **2007**, *126*, 728−734.

(13) Yang, Y.; Ding, Y.; Shi, W.; Ma, F.; Li, Y. The Effects of Amino Group Meta- and Para-Substitution on ESIPT Mechanisms of Amino 2-(2'-Hydroxyphenyl) Benzazole Derivatives. *J. Lumin.* **2020**, *218*, 116836.

(14) Sedgwick, A. C.; Wu, L.; Han, H. H.; Bull, S. D.; He, X. P.; James, T. D.; Sessler, J. L.; Tang, B. Z.; Tian, H.; Yoon, J. Excited-State Intramolecular Proton-Transfer (ESIPT) Based Fluorescence Sensors and Imaging Agents. *Chem. Soc. Rev.* **2018**, *47*, 8842−8880.

(15) Li, Y.; Dahal, D.; Abeywickrama, C. S.; Pang, Y. Progress in Tuning Emission of the Excited-State Intramolecular Proton Transfer (ESIPT)-Based Fluorescent Probes. *ACS Omega* **2021**, *6*, 6547−6553.

(16) Li, J.; Wu, Y.; Xu, Z.; Liao, Q.; Zhang, H.; Zhang, Y.; Xiao, L.; Yao, J.; Fu, H. Tuning the Organic Microcrystal Laser Wavelength of ESIPT-Active Compounds: Via Controlling the Excited Enol- and Keto- Emissions. *J. Mater. Chem. C* **2017**, *5*, 12235−12240.

(17) Sakai, K. I.; Ishikawa, T.; Akutagawa, T. A Blue-White-Yellow Color-Tunable Excited State Intramolecular Proton Transfer (ESIPT) Fluorophore: Sensitivity to Polar-Nonpolar Solvent Ratios. *J. Mater. Chem. C* **2013**, *1*, 7866−7871.

(18) Shukla, A.; Mai, V. T. N.; Divya, V. V.; Suresh, C. H.; Paul, M.; Karunakaran, V.; McGregor, S. K. M.; Allison, I.; Narayanan Unni, K. N.; Ajayaghosh, A.; Namdas, E. B.; Lo, S. C. Amplified Spontaneous Emission from Zwitterionic Excited-State Intramolecular Proton Transfer. *J. Am. Chem. Soc.* **2022**, *144*, 13499−13510.

(19) Wu, K.; Zhang, T.; Wang, Z.; Wang, L.; Zhan, L.; Gong, S.; Zhong, C.; Lu, Z. H.; Zhang, S.; Yang, C. De Novo Design of Excited-State Intramolecular Proton Transfer Emitters via a Thermally Activated Delayed Fluorescence Channel. *J. Am. Chem. Soc.* **2018**, *140*, 8877−8886.

(20) Kumsampao, J.; Chaiwai, C.; Sukpattanacharoen, C.; Nalaoh, P.; Chawanpunyawat, T.; Chasing, P.; Namuangruk, S.; Kungwan, N.; Sudyoadsuk, T.; Promarak, V. Solid-State Fluorophores with Combined Excited-State Intramolecular Proton Transfer-Aggregation-Induced Emission as Efficient Emitters for Electroluminescent Devices. *Adv. Photonics Res.* **2022**, *3*, 2100141.

(21) Mai, V. T. N.; Shukla, A.; Mamada, M.; Maedera, S.; Shaw, P. E.; Sobus, J.; Allison, I.; Adachi, C.; Namdas, E. B.; Lo, S. C. Low Amplified Spontaneous Emission Threshold and Efficient Electroluminescence from a Carbazole Derivatized Excited-State Intramolecular Proton Transfer Dye. *ACS Photonics* **2018**, *5*, 4447−4455.

(22) Mamada, M.; Inada, K.; Komino, T.; Potscavage, W. J.; Nakanotani, H.; Adachi, C. Highly Efficient Thermally Activated Delayed Fluorescence from an Excited-State Intramolecular Proton Transfer System. *ACS Cent. Sci.* **2017**, *3*, 769−777.

(23) Hu, H.; Cheng, X.; Ma, Z.; Sijbesma, R. P.; Ma, Z. Polymer Mechanochromism from Force-Tuned Excited-State Intramolecular Proton Transfer. *J. Am. Chem. Soc.* **2022**, *144*, 9971−9979.
(24) Zhang, G.; Lu, J.; Sabat, M.; Fraser, C. L. Polymorphism and Reversible Mechanochromic Luminescence for Solid-State Difluoroboron Avobenzone. *J. Am. Chem. Soc.* **2010**, *132*, 2160−2162.
(25) Miller, S.; Fanchini, G.; Lin, Y. Y.; Li, C.; Chen, C. W.; Su, W. F.; Chhowalla, M. Investigation of Nanoscale Morphological Changes in Organic Photovoltaics during Solvent Vapor Annealing. *J. Mater. Chem.* **2008**, *18*, 306−312.
(26) Ohisa, S.; Pu, Y. J.; Yamada, N. L.; Matsuba, G.; Kido, J. Molecular Interdiffusion between Stacked Layers by Solution and Thermal Annealing Processes in Organic Light Emitting Devices. *ACS Appl. Mater. Interfaces* **2015**, *7*, 20779−20785.
(27) Ge, J.; Hong, L.; Song, W.; Xie, L.; Zhang, J.; Chen, Z.; Yu, K.; Peng, R.; Zhang, X.; Ge, Z. Solvent Annealing Enables 15.39% Efficiency All-Small-Molecule Solar Cells through Improved Molecule Interconnection and Reduced Non-Radiative Loss. *Adv. Energy Mater.* **2021**, *11*, 2100800.
(28) Skuodis, E.; Bezvikonnyi, O.; Tomkeviciene, A.; Volyniuk, D.; Mimaite, V.; Lazauskas, A.; Bucinskas, A.; Keruckiene, R.; Sini, G.; Grazulevicius, J. V. Aggregation, Thermal Annealing, and Hosting Effects on Performances of an Acridan-Based TADF Emitter. *Org. Electron.* **2018**, *63*, 29−40.
(29) Mondal, A.; Mukhopadhyay, S.; Ahmmed, E.; Banerjee, S.; Zangrando, E.; Chattopadhyay, P. Understanding a Thermoemissive ESIPT-Based Solid-State off-on Switch as a Dual-Channel Chemosensor in Solid and Solution Phases: Detailed Experimental and Theoretical Study. *J. Phys. Chem. C* **2020**, *124*, 18181−18193.
(30) Li, A.; Liu, H.; Song, C.; Geng, Y.; Xu, S.; Zhang, H.; Zhang, H.; Cui, H.; Xu, W. Flexible Control of Excited State Transition under Pressure/Temperature: Distinct Stimuli-Responsive Behaviours of Two ESIPT Polymorphs. *Mater. Chem. Front.* **2019**, *3*, 2128−2136.
(31) Gayathri, P.; Kanagajothi, K.; Nag, P.; Anand, N.; Reddy, V. S.; Moon, D.; Anthony, S. P.; Madhu, V. Symmetrical and Unsymmetrical Thiazole-Based ESIPT Derivatives: The Highly Selective Fluorescence Sensing of Cu2+ and Structure-Controlled Reversible Mechanofluorochromism. *CrystEngComm* **2021**, *23*, 6769−6777.
(32) Chanda, K.; Rajasekhar, S.; Maiti, B. A Decade Update on Benzoxazoles, a Privileged Scaffold in Synthetic Organic Chemistry. *Synlett* **2017**, *28*, 521−541.
(33) Passemard, S.; Szabó, L.; Noverraz, F.; Montanari, E.; Gonelle-Gispert, C.; Bühler, L. H.; Wandrey, C.; Gerber-Lemaire, S. Synthesis Strategies to Extend the Variety of Alginate-Based Hybrid Hydrogels for Cell Microencapsulation. *Biomacromolecules* **2017**, *18*, 2747−2755.
(34) Chai, J.-D.; Head-Gordon, M. Long-Range Corrected Hybrid Density Functionals with Damped Atom−Atom Dispersion Corrections. *Phys. Chem. Chem. Phys.* **2008**, *10*, 6615−6620.
(35) Frisch, M. J.; Trucks, G. W.; Schlegel, H. B.; Scuseria, G. E.; Robb, M. A.; Cheeseman, J. R.; Scalmani, G.; Barone, V.; Petersson, G. A.; Nakatsuji, H.; et al. *Gaussian 16*, Revision C.01: Gaussian, Inc.: Wallingford CT, 2016. https://gaussian.com/citation (accessed 04 24, 2022).
(36) Miertuš, S.; Scrocco, E.; Tomasi, J. Electrostatic Interaction of a Solute with a Continuum. A Direct Utilizaion of AB Initio Molecular Potentials for the Prevision of Solvent Effects. *Chem. Phys.* **1981**, *55*, 117−129.
(37) Cossi, M.; Barone, V.; Cammi, R.; Tomasi, J. Ab Initio Study of Solvated Molecules: A New Implementation of the Polarizable Continuum Model. *Chem. Phys. Lett.* **1996**, *255*, 327−335.
(38) Lu, T.; Chen, F. Multiwfn: A multifunctional wavefunction analyzer. *J. Comput. Chem.* **2012**, *33*, 580−592.
(39) Pettersen, E. F.; Goddard, T. D.; Huang, C. C.; Meng, E. C.; Couch, G. S.; Croll, T. I.; Morris, J. H.; Ferrin, T. E. UCSF ChimeraX: Structure Visualization for Researchers, Educators, and Developers. *Protein Sci.* **2021**, *30*, 70−82.
(40) Goddard, T. D.; Huang, C. C.; Meng, E. C.; Pettersen, E. F.; Couch, G. S.; Morris, J. H.; Ferrin, T. E. UCSF ChimeraX: Meeting Modern Challenges in Visualization and Analysis. *Protein Sci.* **2018**, *27*, 14−25.
(41) McLean, A. D.; Chandler, G. S. Contracted Gaussian Basis Sets for Molecular Calculations. I. Second Row Atoms, Z=11−18. *J. Chem. Phys.* **1980**, *72*, 5639−5648.
(42) Montalbetti, C. A. G. N.; Falque, V. Amide Bond Formation and Peptide Coupling. *Tetrahedron* **2005**, *61*, 10827−10852.
(43) Coelho, F. L.; Rodembusch, F. S.; Campo, L. F. Synthesis, Characterization and Photophysics of New Photoactive ESIPT Lipophilic Dyes. Partition Experiments with Different Composed Liposomes. *Dyes Pigments* **2014**, *110*, 134−142.
(44) Conti, P.; Tamborini, L.; Pinto, A.; Sola, L.; Ettari, R.; Mercurio, C.; De Micheli, C. Design and Synthesis of Novel Isoxazole-Based HDAC Inhibitors. *Eur. J. Med. Chem.* **2010**, *45*, 4331−4338.
(45) Rahm, M.; Christe, K. O. Quantifying the Nature of Lone Pair Domains. *ChemPhysChem* **2013**, *14*, 3714−3725.
(46) Mishra, V. R.; Ghanavatkar, C. W.; Sekar, N. Towards NIR-Active Hydroxybenzazole (HBX)-Based ESIPT Motifs: A Recent Research Trend. *ChemistrySelect* **2020**, *5*, 2103−2113.
(47) Manne, S. R.; Luna, O.; Acosta, G. A.; Royo, M.; El-Faham, A.; Orosz, G.; De La Torre, B. G.; Albericio, F. Amide Formation: Choosing the Safer Carbodiimide in Combination with OxymaPure to Avoid HCN Release. *Org. Lett.* **2021**, *23*, 6900−6904.
(48) Valeur, E.; Bradley, M. Amide Bond Formation: Beyond the Myth of Coupling Reagents. *Chem. Soc. Rev.* **2009**, *38*, 606−631.
(49) Frizon, T. E. A.; Salla, C. A. M.; Grillo, F.; Rodembusch, F. S.; Câmara, V. S.; Silva, H. C.; Zapp, E.; Junca, E.; Galetto, F. Z.; de Costa, A. M.; et al. ESIPT-Based Benzazole-Pyromellitic Diimide Derivatives. A Thermal, Electrochemical, and Photochemical Investigation. *Spectrochim. Acta Mol. Biomol. Spectrosc.* **2023**, *288*, 122050.
(50) Berbigier, J. F.; Teixeira Alves Duarte, L. G.; Zawacki, M. F.; de Araújo, B. B.; Moura Santos, C. d.; Atvars, T. D. Z.; Gonçalves, P. F. B.; Petzhold, C. L.; Rodembusch, F. S.; Rodembusch, F. S. ATRP Initiators Based on Proton Transfer Benzazole Dyes: Solid-State Photoactive Polymer with Very Large Stokes Shift. *ACS Appl. Polym. Mater.* **2020**, *2*, 1406−1416.
(51) Munch, M.; Curtil, M.; Vérité, P. M.; Jacquemin, D.; Massue, J.; Ulrich, G. Ethynyl-Tolyl Extended 2-(2′-Hydroxyphenyl)-Benzoxazole Dyes: Solution and Solid-State Excited-State Intramolecular Proton Transfer (ESIPT) Emitters. *Eur. J. Org Chem.* **2019**, 1134−1144.
(52) Pariat, T.; Stoerkler, T.; Diguet, C.; Laurent, A. D.; Jacquemin, D.; Ulrich, G.; Massue, J. Dual Solution-/Solid-State Emissive Excited-State Intramolecular Proton Transfer (ESIPT) Dyes: A Combined Experimental and Theoretical Approach. *J. Org. Chem.* **2021**, *86*, 17606−17619.
(53) Gierschner, J.; Shi, J.; Milián-Medina, B.; Roca-Sanjuán, D.; Varghese, S.; Park, S. Y. Luminescence in Crystalline Organic Materials: From Molecules to Molecular Solids. *Adv. Opt. Mater.* **2021**, *9*, 2002251.
(54) Ji, S.; Yang, J.; Yang, Q.; Liu, S.; Chen, M.; Zhao, J. Tuning the Intramolecular Charge Transfer of Alkynylpyrenes: Effect on Photophysical Properties and Its Application in Design of OFF-ON Fluorescent Thiol Probes. *J. Org. Chem.* **2009**, *74*, 4855−4865.
(55) Jung, M.; Yoon, Y.; Park, J. H.; Cha, W.; Kim, A.; Kang, J.; Gautam, S.; Seo, D.; Cho, J. H.; Kim, H.; et al. Nanoscopic Management of Molecular Packing and Orientation of Small Molecules by a Combination of Linear and Branched Alkyl Side Chains. *ACS Nano* **2014**, *8*, 5988−6003.
(56) Yao, X.; Shao, W.; Xiang, X.; Xiao, W. J.; Liang, L.; Zhao, F. G.; Ling, J.; Lu, Z.; Li, J.; Li, W. S. Side Chain Engineering on a Small Molecular Semiconductor: Balance between Solubility and Performance by Choosing Proper Positions for Alkyl Side Chains. *Org. Electron.* **2018**, *61*, 56−64.
(57) Mei, J.; Bao, Z. Side Chain Engineering in Solution-Processable Conjugated Polymers. *Chem. Mater.* **2014**, *26*, 604−615.

(58) Inoue, S.; Minemawari, H.; Tsutsumi, J.; Chikamatsu, M.; Yamada, T.; Horiuchi, S.; Tanaka, M.; Kumai, R.; Yoneya, M.; Hasegawa, T. Effects of Substituted Alkyl Chain Length on Solution-Processable Layered Organic Semiconductor Crystals. *Chem. Mater.* **2015**, *27*, 3809−3812.
(59) Zhang, Z.; Chen, Y. A.; Hung, W. Y.; Tang, W. F.; Hsu, Y. H.; Chen, C. L.; Meng, F. Y.; Chou, P. T. Control of the Reversibility of Excited-State Intramolecular Proton Transfer (ESIPT) Reaction: Host-Polarity Tuning White Organic Light Emitting Diode on a New Thiazolo[5,4-d]Thiazole ESIPT System. *Chem. Mater.* **2016**, *28*, 8815−8824.
(60) Rajamalli, P.; Senthilkumar, N.; Huang, P. Y.; Ren-Wu, C. C.; Lin, H. W.; Cheng, C. H. New Molecular Design Concurrently Providing Superior Pure Blue, Thermally Activated Delayed Fluorescence and Optical Out-Coupling Efficiencies. *J. Am. Chem. Soc.* **2017**, *139*, 10948−10951.
(61) Qiu, X.; Xu, Y.; Wang, C.; Hanif, M.; Zhou, J.; Zeng, C.; Li, Y.; Jiang, Q.; Zhao, R.; Hu, D.; Ma, Y. Synergistic Effects of Hydrogen Bonds and the Hybridized Excited State Observed for High-Efficiency, Deep-Blue Fluorescent Emitters with Narrow Emission in OLED Applications. *J. Mater. Chem. C* **2019**, *7*, 5461−5467.
(62) Bin, H.; Gao, L.; Zhang, Z. G.; Yang, Y.; Zhang, Y.; Zhang, C.; Chen, S.; Xue, L.; Yang, C.; Xiao, M.; et al. 11.4% Efficiency Non-Fullerene Polymer Solar Cells with Trialkylsilyl Substituted 2D-Conjugated Polymer as Donor. *Nat. Commun.* **2016**, *7*, 13651.
(63) Li, G.; Shrotriya, V.; Huang, J.; Yao, Y.; Moriarty, T.; Emery, K.; Yang, Y. High-Efficiency Solution Processable Polymer Photovoltaic Cells by Self-Organization of Polymer Blends. *Nat. Mater.* **2005**, *4*, 864−868.
(64) Erb, T.; Zhokhavets, U.; Gobsch, G.; Raleva, S.; Stühn, B.; Schilinsky, P.; Waldauf, C.; Brabec, C. J. Correlation between Structural and Optical Properties of Composite Polymer/Fullerene Films for Organic Solar Cells. *Adv. Funct. Mater.* **2005**, *15*, 1193−1196.
(65) Chen, D. Y.; Liu, W.; Zheng, C. J.; Wang, K.; Li, F.; Tao, S. L.; Ou, X. M.; Zhang, X. H. Isomeric Thermally Activated Delayed Fluorescence Emitters for Color Purity-Improved Emission in Organic Light-Emitting Devices. *ACS Appl. Mater. Interfaces* **2016**, *8*, 16791−16798.
(66) Yablonovitch, E. Statistical Ray Optics. *J. Opt. Soc. Am.* **1982**, *72*, 899−907.
(67) Tsutsui, Y.; Zhang, W.; Ghosh, S.; Sakurai, T.; Yoshida, H.; Ozaki, M.; Akutagawa, T.; Seki, S. Electrically Switchable Amplified Spontaneous Emission from Liquid Crystalline Phase of an AIEE-Active ESIPT Molecule. *Adv. Opt. Mater.* **2020**, *8*, 1902158.
(68) Yan, C. C.; Wang, X. D.; Liao, L. S. Organic Lasers Harnessing Excited State Intramolecular Proton Transfer Process. *ACS Photonics* **2020**, *7*, 1355−1366.
(69) Manley, E. F.; Strzalka, J.; Fauvell, T. J.; Marks, T. J.; Chen, L. X. In Situ Analysis of Solvent and Additive Effects on Film Morphology Evolution in Spin-Cast Small-Molecule and Polymer Photovoltaic Materials. *Adv. Energy Mater.* **2018**, *8*, 1800611.
(70) Lee, W. Y.; Giri, G.; Diao, Y.; Tassone, C. J.; Matthews, J. R.; Sorensen, M. L.; Mannsfeld, S. C. B.; Chen, W. C.; Fong, H. H.; Tok, J. B. H.; et al. Effect of Non-Chlorinated Mixed Solvents on Charge Transport and Morphology of Solution-Processed Polymer Field-Effect Transistors. *Adv. Funct. Mater.* **2014**, *24*, 3524−3534.
(71) Ma, R.; Yang, T.; Xiao, Y.; Liu, T.; Zhang, G.; Luo, Z.; Li, G.; Lu, X.; Yan, H.; Tang, B. Air-Processed Efficient Organic Solar Cells from Aromatic Hydrocarbon Solvent without Solvent Additive or Post-Treatment: Insights into Solvent Effect on Morphology. *Energy Environ. Mater.* **2022**, *5*, 977−985.

https://doi.org/10.1021/acs.jpcc.3c04543
J. Phys. Chem. C 2023, 127, 17624−17636